Journal of Power Sources 182 (2008) 503–509

Contents lists available at ScienceDirect

Journal of Power Sources

journal homepage: www.elsevier.com/locate/jpowsour

Preparation and properties of $Ba_xSr_{1-x}Co_yFe_{1-y}O_{3-\delta}$ cathode material for intermediate temperature solid oxide fuel cells

Hailei Zhao[a,c,*], Wei Shen[a], Zhiming Zhu[b], Xue Li[a], Zhifeng Wang[a]

[a] *Department of Inorganic Nonmetallic Materials, University of Science and Technology Beijing, Beijing 100083, China*
[b] *Department of Mechanical Engineering, Tsinghua University, Beijing 100084, China*
[c] *Beijing Key Lab of New Energy Materials and Technology, Beijing 100083, China*

ARTICLE INFO

Article history:
Received 9 February 2008
Received in revised form 13 April 2008
Accepted 14 April 2008
Available online 29 April 2008

Keywords:
BSCF
Electrical conductivity
Cathode performance
SOFCs

ABSTRACT

$Ba_xSr_{1-x}Co_yFe_{1-y}O_{3-\delta}$ (BSCF) materials with perovskite structure were synthesized via solid-state reaction. Their structural characteristics, electrical-conduction behavior and cathode performance were investigated. Compared to A-site elements, B-site elements show a wide solid-solution range in BSCF. The electrical-conduction behavior of BSCF obeys the small polaron-hopping mechanism. An increase of Ba or Co content in the BSCF samples results in a decrease of electrical conductivity, which is mainly attributable to the preferential existence of B^{3+} rather than B^{4+} in Ba- or Co-rich samples. At the same time, this leads to increases in the lattice parameter *a* and the number of oxygen vacancies. BSCF samples with high Ba content show a high structural stability (high oxygen-loss temperature). $Ba_{0.6}Sr_{0.4}Co_{0.8}Fe_{0.2}O_{3-\delta}$ and $Ba_{0.5}Sr_{0.5}Co_{0.8}Fe_{0.2}O_{3-\delta}$ materials present good thermal-cycling stability of the electrical conductivity. Compared with $Ba_{0.5}Sr_{0.5}Co_{0.8}Fe_{0.2}O_{3-\delta}$, $Ba_{0.6}Sr_{0.4}Co_{0.8}Fe_{0.2}O_{3-\delta}$ exhibits a better cathode performance in a $Ce_{0.8}Gd_{0.2}O_{2-\delta}$ (GDC)-supported half cell. The cell performance can be improved by introducing a certain amount of GDC electrolyte into the BSCF cathode material.

1. Introduction

Solid oxide fuel cells (SOFCs), which combine the benefits of environmentally friendly power generation with high efficiency and fuel flexibility, are attracting more and more attention. A traditional SOFC demands high-temperature (800–1000 °C) operation, which causes many problems in sealing, material compatibility and fabrication cost [1,2]. So it is necessary to reduce the operating temperature in order to improve the material compatibility and practical applications. The most common cathode material, Sr-doped $LaMnO_3$ (LSM), cannot meet the cathodic requirements when the working temperature is reduced because of its low ionic conductivity and poor catalysis [3]. Therefore, new cathode materials to replace LSM must be explored for intermediate-temperature use. Perovskite cobalt oxides ($ACoO_3$) are the most promising candidates for cathodes in terms of their electrical conductivity and catalytic performance at intermediate temperature (500–800 °C). The use of lanthanum cobalt oxide materials as possible cathodes has also been widely investigated in recent years. The B site is often doped with Fe to partially replace Co in order to adjust the thermal-expansion coefficient and long-term stability. $La_{0.6}Sr_{0.4}Co_{0.8}Fe_{0.2}O_{3-\delta}$ is considered to be the optimal cathode material in the system $La_{1-x}Sr_xCo_{1-y}Fe_yO_{3-\delta}$ [4–6].

Shao and Haile [7] replaced the trivalent rare-earth element with a divalent alkaline-earth element to obtain the novel cathode material, $Ba_{0.5}Sr_{0.5}Co_{0.8}Fe_{0.2}O_{3-\delta}$. This material possesses a high rate of oxygen diffusion and shows excellent cell performance with a ceria-based electrolyte at intermediate temperatures. In addition, further investigation demonstrated that it is ideally suited for single-chamber fuel-cell operation, which could avoid the difficulty of sealing. The use of a cheap alkaline-earth element would also promote widespread business implementation of SOFCs. Because of these advantages, this new cathode material, $Ba_{0.5}Sr_{0.5}Co_{0.8}Fe_{0.2}O_{3-\delta}$, has received a great deal of attention. Zhu et al. [8] and Peña-Martínez et al. [9] studied the material compatibility of $Ba_{0.5}Sr_{0.5}Co_{0.8}Fe_{0.2}O_{3-\delta}$ with YSZ (8 mol% yttria-stabilized zirconia), GDC ($Ce_{0.8}Gd_{0.2}O_{2-\delta}$) and LSGM ($La_{0.9}Sr_{0.1}Ga_{0.8}Mg_{0.2}O_{2.85}$). Many cathode materials based on $Ba_{0.5}Sr_{0.5}Co_{0.8}Fe_{0.2}O_{3-\delta}$ have now been evaluated [10–12]. These researches were mainly focused on the cell performance with $Ba_{0.5}Sr_{0.5}Co_{0.8}Fe_{0.2}O_{3-\delta}$ as cathode material. These reports

* Corresponding author at: Department of Inorganic Nonmetallic Materials, University of Science and Technology Beijing, Beijing 100083, China.
Tel.: +86 10 62334863; fax: +86 10 62332570.
E-mail address: hlzhao@mater.ustb.edu.cn (H. Zhao).

0378-7753/$ – see front matter © 2008 Elsevier B.V. All rights reserved.
doi:10.1016/j.jpowsour.2008.04.046

barely referred to the electrical conductivity and conduction mechanisms of this cathode material, which are crucial to the cathode performance. Moreover, the effects of the doping level of A/B-site elements on the conduction behavior, and hence on the cell output power, have not been investigated. In present work, the solid-solution ranges of the A/B-site elements in the system $Ba_xSr_{1-x}Co_yFe_{1-y}O_{3-\delta}$ (BSFC) are examined. The emphasis is put on the effects of the composite elements of BSCF materials on their electrical conductivity and conduction behavior. The charge-compensation mechanism and the electronic- and ionic-conduction mechanisms are also discussed. Finally, the performance of a cathode with the optimized composition $Ba_{0.6}Sr_{0.4}Co_{0.8}Fe_{0.2}O_{3-\delta}$ is compared with the widely studied composition $Ba_{0.5}Sr_{0.5}Co_{0.8}Fe_{0.2}O_{3-\delta}$ to widen the research on the BSFC series of materials.

2. Experimental

The compounds $Ba_xSr_{1-x}Co_yFe_{1-y}O_{3-\delta}$ ($0.2 \le x \le 0.7$, $0 \le y \le 1$) were synthesized by solid-state reactions in air at 1000 °C for 6 h with $BaCO_3$, $SrCO_3$, $CoCO_3$ and Fe_2O_3 as raw materials, which had been ball-milled for 4 h in alcohol. X-ray diffraction (XRD, Rigaku D/max-A X-ray diffractometer) with Cu Kα radiation was used to determine the phase of the compound and to obtain the lattice parameters of the material structure. The composite powder was uniaxially pressed (~150 MPa) into bars (40 mm × 7 mm × 3 mm) and then sintered at different temperatures for 8 h to obtain dense samples for measurement of the density and electrical conductivity. The sintering temperature for $Ba_{0.5}Sr_{0.5}Co_yFe_{1-y}O_{3-\delta}$ and $Ba_xSr_{1-x}Co_{0.8}Fe_{0.2}O_{3-\delta}$ (x = 0.4, 0.5) was 1200 °C, while that for $Ba_xSr_{1-x}Co_{0.8}Fe_{0.2}O_{3-\delta}$ (x = 0.3, 0.6) was 1140 °C. The heating and cooling rates were 2 °C min^{-1}. The microstructural characteristics of the samples were observed by scanning electron microscopy (SEM, Cambridge S250-MK2). The bulk densities of the BSCF samples were determined by Archimedes' method using de-ionized water as the liquid medium.

The conductivity was measured by a standard four-terminal DC method [13–15] under static air conditions from 300 to 1000 °C. This method is suitable for materials with moderate or high conductivity. The heating rate was 5 °C min^{-1} for all samples. The electrical-conductivity data were taken every 50 °C after holding at each temperature for at least 15 min to equilibrate until no significant change in measured value was observed. Some samples were cooled in air and then heated to the final temperature twice to measure the electrical conductivity for the evaluation of the thermal-cycling stability of BSCF.

The half cell was packed by using a GDC electrolyte disc as the cell structural support and Pt paste as the anode and electrical collector. The GDC powder was successfully synthesized at 1300 °C for 5 h from high purity CeO_2 and Gd_2O_3 by solid-state reaction. Dense GDC films 280 μm thick and 10 mm diameter were obtained by uniaxially pressing the synthesized powder at 75 MPa and then sintering the green body at 1550 °C for 5 h. Screen printing was used to deposit the cathode on the electrolyte. The cathode slurry was prepared by mixing the cathode materials with active carbon as the pore-forming reagent and ethylic cellulose solution. The Pt paste was coated onto both sides of the cell film as the current collector. The single cells were calcined at 850 °C for 3 h to enhance the combination between the electrodes and electrolyte. The cell tests were performed with moistened pure H_2 as the fuel at a flow rate of 30 ml min^{-1} and static air as the oxidant at intermediate temperatures (500–700 °C). The *I–V* plots were obtained by changing the external resistor.

3. Results and discussion

3.1. Phase and lattice-structure development

A series of $Ba_xSr_{1-x}Co_yFe_{1-y}O_{3-\delta}$ ($0.2 \le x \le 0.7$, $0 \le y \le 1$) materials was synthesized and the solid solution of A/B-site elements in the BSCF perovskite structure was examined. In order to determine the synthesis temperature of $Ba_{0.5}Sr_{0.5}Co_{0.8}Fe_{0.2}O_{3-\delta}$, a mixture of raw materials with the designed chemical composition was calcined at 900, 1000 and 1100 °C for 6 h, respectively. Fig. 1 presents the XRD patterns of calcined $Ba_{0.5}Sr_{0.5}Co_{0.8}Fe_{0.2}O_{3-\delta}$ powder. After calcining at 900 °C, the sample shows the main peaks of the perovskite structure with a small amount of $BaCoO_3$ impurity. This impurity disappears and a single cubic perovskite structure forms when the calcination temperature is raised to 1000 °C. The peak intensity increases remarkably after higher temperature calcination (1100 °C), indicating the high crystallinity of the synthesized $Ba_{0.5}Sr_{0.5}Co_{0.8}Fe_{0.2}O_{3-\delta}$ powder. Based on these results, the synthesis condition for the $Ba_{0.5}Sr_{0.5}Co_yFe_{1-y}O_{3-\delta}$ compounds with different y values (y = 0, 0.2, 0.4, 0.6, 0.8, 1) was set as 1000 °C for 6 h in air to investigate the solid-solution range of B-site elements in BSCF. The XRD data indicate that all the prepared $Ba_{0.5}Sr_{0.5}Co_yFe_{1-y}O_{3-\delta}$ samples have a single cubic perovskite phase except the sample with y = 1, which shows a hexagonal structure (see Fig. 2). It is reasonable to state that the solid-solution

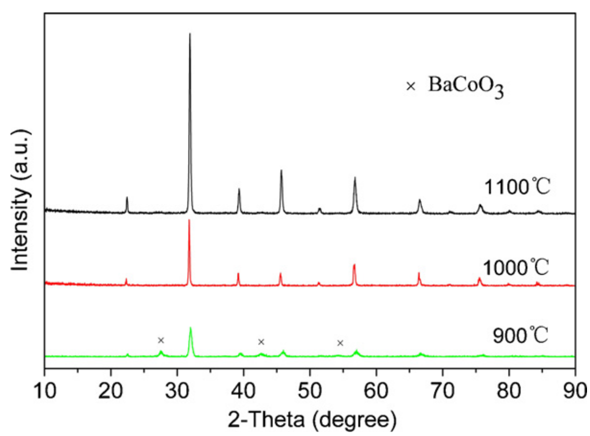

Fig. 1. XRD patterns of $Ba_{0.5}Sr_{0.5}Co_{0.8}Fe_{0.2}O_{3-\delta}$ samples sintered at different temperatures.

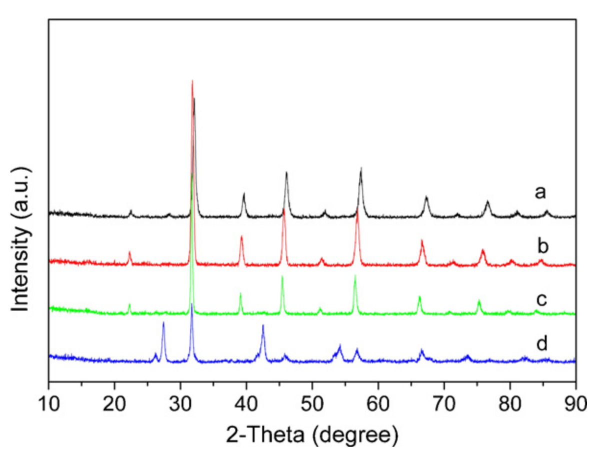

Fig. 2. XRD patterns of $Ba_{0.5}Sr_{0.5}Co_yFe_{1-y}O_{3-\delta}$ samples sintered at 1000 °C: (a) y = 0; (b) y = 0.4; (c) y = 0.8; and (d) y = 1.

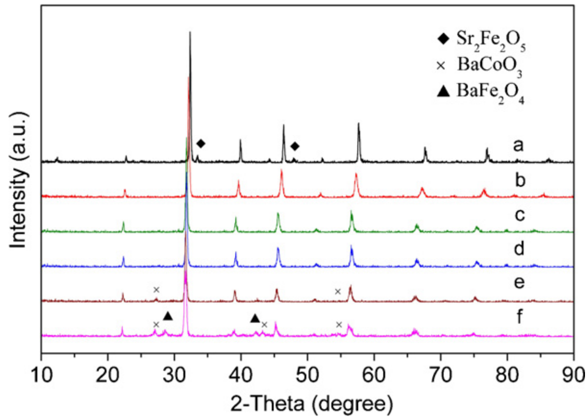

Fig. 3. XRD patterns of $Ba_xSr_{1-x}Co_{0.8}Fe_{0.2}O_{3-\delta}$ sintered at 1000 °C: (a) x = 0.2; (b) x = 0.3; (c) x = 0.4; (d) x = 0.5; (e) x = 0.6; and (f) x = 0.7.

limit of Co in this series of cubic perovskite materials is more than 80 mol% at 1000 °C.

$Ba_xSr_{1-x}Co_{0.8}Fe_{0.2}O_{3-\delta}$ samples with different A-site compositions ($0.2 \le x \le 0.7$) were also synthesized at 1000 °C for 6 h and the phase structural characteristics were examined. The results are shown in Fig. 3. The pure cubic perovskite phase can be obtained in the compounds $Ba_xSr_{1-x}Co_{0.8}Fe_{0.2}O_{3-\delta}$ when $0.3 \le x \le 0.5$; however, a small amount of impurity is detected when x = 0.2, 0.6 and 0.7. On increasing the calcination temperature to 1140 °C, the sample with x = 0.6 exhibits a pure perovskite structure without any impurity, while a trace amount of impurity is still detected in the sample with x = 0.2, as shown in Fig. 4. For the sample with x = 0.7, a certain amount of impurity still remains when it is heated to 1100 °C and a large amount of liquid is formed when heated to 1140 °C. Therefore, it is reasonable to state that $Ba_{0.5}Sr_{0.5}Co_yFe_{1-y}O_{3-\delta}$ with a single cubic perovskite phase can be obtained at 1000 °C when $0 \le y \le 0.8$. The solution range of barium in $Ba_xSr_{1-x}Co_{0.8}Fe_{0.2}O_{3-\delta}$ can be extended from $0.3 \le x \le 0.5$ to $0.3 \le x \le 0.6$ by increasing the temperature from 1000 to 1140 °C.

Tables 1 and 2 list the lattice parameters and relative densities of $Ba_xSr_{1-x}Co_yFe_{1-y}O_{3-\delta}$ ($0.3 \le x \le 0.6, 0 \le y \le 0.8$) samples. The lattice parameter a increases with increasing Co or Ba content. The ionic radii of Co^{n+} are somewhat smaller than those of Fe^{n+} with the same valence ($r_{Fe^{3+}} = 0.79$ Å, $r_{Co^{3+}} = 0.75$ Å, $r_{Fe^{4+}} = 0.73$ Å, $r_{Co^{4+}} = 0.67$ Å) [16], so the equivalent substitution of Co for Fe cannot bring about this variation of lattice parameter a. This implies that Co ions in BSCF materials may take the Co^{3+} state rather than the Co^{4+} state, and the Co^{3+} ions replace parts of Fe^{4+} ions leading to expansion of the lattice. This is consistent with the reported data [6], which suggested that acceptor dopants might be preferentially compensated by forming Fe^{4+} ions instead of Co^{4+} ions in the $La_{0.8}Sr_{0.2}Co_{1-y}Fe_yO_3$ system. The incorporation of Co leads to the decrease of average valence of B-site elements, this may be compensated by the formation of oxygen vacancies. Increasing the Ba content also results in this expansion because of the larger ionic radius of Ba^{2+} (1.75 Å) compared to that of Sr^{2+} (1.58 Å) [16]. The relative densities of the $Ba_{0.5}Sr_{0.5}Co_yFe_{1-y}O_{3-\delta}$ ($0 \le y \le 0.8$) samples are very similar, but for that of $Ba_xSr_{1-x}Co_{0.8}Fe_{0.2}O_{3-\delta}$ ($0.3 \le x \le 0.6$), the samples with a Ba/Sr ratio close to 1 are easy to densify.

3.2. Dependence of electrical conductivity on B-site composition

The results of four-probe DC electrical-conductivity measurements on $Ba_{0.5}Sr_{0.5}Co_yFe_{1-y}O_{3-\delta}$ (y = 0.2, 0.4, 0.6, 0.8) samples in air from 300 to 800 °C are shown in Fig. 5. All the samples have the same tendency in the temperature dependence of their electrical conductivity. The electrical conductivity of each sample increases with temperature through a maximum, then decreases. The temperature of the maximal electrical conductivity shifts from approximately 500 to 550 °C as the Co content decreases from y = 0.6 to y = 0.2. The sample with y = 0.8 is an exception. At low temperatures, the electrical conductivity of $Ba_{0.5}Sr_{0.5}Co_yFe_{1-y}O_{3-\delta}$ decreases with Co content, while it increases with Co content at high temperatures. This transformation is related to the charge compensation of the material system.

For BSCF materials, the A-site elements are both divalent alkaline-earth ions, which according to the electrovalent equilibrium would cause two results [17]. On one hand, the B-site transition-metal ions change from trivalent to tetravalent, which would introduce electronic conductivity (electron holes by $B^{4+}_{B^{3+}}{}^{\bullet}$). On the other hand, some lattice oxygen is lost as charge compensation, which will lead to the generation of an oxygen vacancy ($V_O^{\bullet\bullet}$), the materials thus possessing ionic conductivity. Because the ionic conductivity of mixed ionic and electronic conductors (MIECs) is usually several orders of magnitude lower than the electronic conductivity [18,19], it is reasonable to assume that the measured values mainly refer to the electronic conductivity. The temperature dependence of the electrical conductivity of $Ba_{0.5}Sr_{0.5}Co_yFe_{1-y}O_{3-\delta}$ shows a semiconducting behavior, which can be described by a p-type small polaron-hopping mechanism [19], i.e. the charge carriers hop between $B_B^{\bullet}$–O–$B_B^{\times}$.

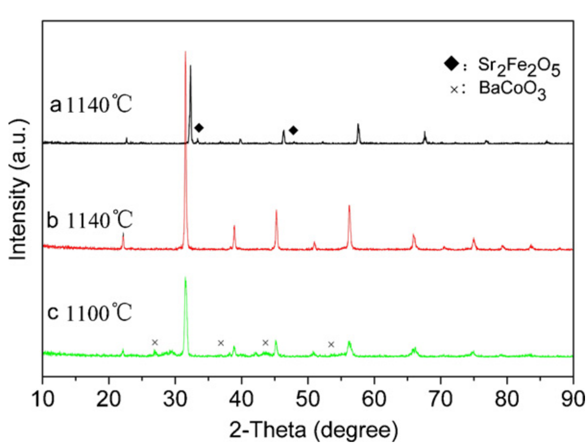

Fig. 4. XRD patterns of $Ba_xSr_{1-x}Co_{0.8}Fe_{0.2}O_{3-\delta}$ samples sintered at different temperatures: (a) x = 0.2; (b) x = 0.6; and (c) x = 0.7.

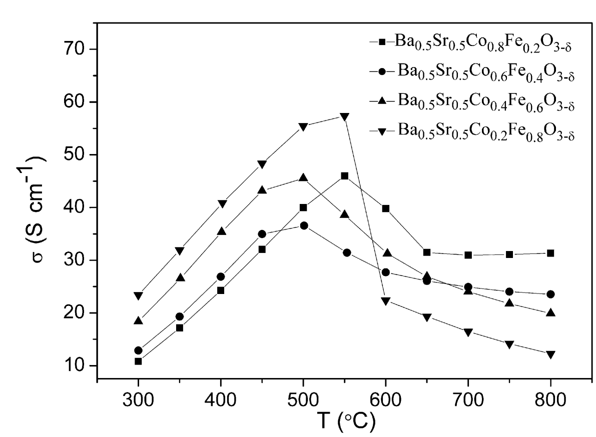

Fig. 5. Temperature dependence of electrical conductivity of $Ba_{0.5}Sr_{0.5}Co_yFe_{1-y}O_{3-\delta}$ samples with different B-site compositions.

Table 1
Lattice parameters and relative densities of samples with different B-site compositions

Sample	Lattice parameter, *a* (Å)	Theoretical density ($g\,cm^{-3}$)	Volume density ($g\,cm^{-3}$)	Relative density (%)
$Ba_{0.5}Sr_{0.5}Co_{0.2}Fe_{0.8}O_{3-\delta}$	3.950	5.844	5.255	89.93
$Ba_{0.5}Sr_{0.5}Co_{0.4}Fe_{0.6}O_{3-\delta}$	3.967	5.788	5.199	89.82
$Ba_{0.5}Sr_{0.5}Co_{0.6}Fe_{0.4}O_{3-\delta}$	3.982	5.739	5.127	89.34
$Ba_{0.5}Sr_{0.5}Co_{0.8}Fe_{0.2}O_{3-\delta}$	3.989	5.725	5.051	88.23

Table 2
Lattice parameters and relative densities of samples with different A-site compositions

Sample	Lattice parameter, *a* (Å)	Theoretical density ($g\,cm^{-3}$)	Volume density ($g\,cm^{-3}$)	Relative density (%)
$Ba_{0.3}Sr_{0.7}Co_{0.8}Fe_{0.2}O_{3-\delta}$	3.936	5.689	4.618	81.18
$Ba_{0.4}Sr_{0.6}Co_{0.8}Fe_{0.2}O_{3-\delta}$	3.970	5.675	4.914	86.59
$Ba_{0.5}Sr_{0.5}Co_{0.8}Fe_{0.2}O_{3-\delta}$	3.989	5.725	5.051	88.23
$Ba_{0.6}Sr_{0.4}Co_{0.8}Fe_{0.2}O_{3-\delta}$	4.005	5.783	4.745	82.06

For doped semiconductors, the temperature dependence of the electrical conductivity can be expressed as

$$\sigma = \left(\frac{A}{T}\right) \exp\left(-\frac{E_a}{kT}\right) \quad (1)$$

The pre-exponential factor A is a material constant, and E_a is the hopping activation energy [19–21]. Based on this equation, two different temperature dependences may be expected. At low temperatures, the electrical conductivity is mainly determined by the exponential term and it increases with temperature. At high temperatures, the pre-exponential factor (A/T) starts to dominate the temperature dependence, and the electrical conductivity decreases with increasing temperature. A maximum value for the electrical conductivity will occur at a characteristic temperature (T_{max}):

$$E_a = kT_{max} \quad (2)$$

As mentioned above, the lattice oxygen of doped semiconductors may be lost at high temperatures, which will result in the generation of oxygen vacancies and the annihilation of electron holes, as expressed in Eq. (3). The latter will lead to a decrease in the concentration of electron holes and thus in the electrical conductivity. The temperature at which lattice oxygen is lost is usually lower than the characteristic temperature T_{max} of doped semiconductors [19].

$$O_O^{\times} = \frac{1}{2}O_2(g) + V_O^{\bullet\bullet} + 2e' \quad (3)$$

Fig. 5 shows the expected change in behavior of the electrical conductivity: it increases at lower temperatures and decreases at higher temperatures. There are different transition temperatures (T'_{max}) for $Ba_{0.5}Sr_{0.5}Co_yFe_{1-y}O_{3-\delta}$ samples with different compositions. T'_{max} increases with the Fe content in $Ba_{0.5}Sr_{0.5}Co_yFe_{1-y}O_{3-\delta}$, except for the sample with $y = 0.8$. The transition temperatures of electrical conductivity (T'_{max}) in Fig. 5 should correspond to the loss of lattice oxygen but not to the T_{max} expressed in Eq. (2).

At low temperatures, the electrical conductivity of the samples increases with the Fe content in $Ba_{0.5}Sr_{0.5}Co_yFe_{1-y}O_{3-\delta}$. According to the charge-compensation mechanism, the concentration of electron holes equals $[B^{4+}_{B^{3+}}{}^\bullet]$. It is easier to form B^{4+} for Fe ions than for Co [5,6]. Therefore, the concentration of electron holes is relatively high in Fe-rich samples of $Ba_{0.5}Sr_{0.5}Co_yFe_{1-y}O_{3-\delta}$, which results in their high electrical conductivity. For Co-rich samples $[B^{4+}_{B^{3+}}{}^\bullet]$ is relatively low, and more $V_O^{\bullet\bullet}$ are needed to maintain the electrostatic neutrality. Because of the low mobility of oxygen ions, the ionic conductivity is several orders of magnitude lower than the electronic conductivity. As a result, Co-rich samples show a low conductivity. At high temperatures, there is a reverse dependence of electrical conductivity on composition: Fe-rich samples exhibit low electrical conductivity. This may be due to the rapid oxygen loss of these samples at high temperatures, as expressed in Eq. (3). To confirm this hypothesis, further investigation is undoubtedly necessary.

3.3. Dependence of electrical conductivity on A-site composition

The electrical conductivity of $Ba_xSr_{1-x}Co_{0.8}Fe_{0.2}O_{3-\delta}$ ($0.3 \le x \le 0.6$) samples with different A-site compositions was investigated. The results are shown in Fig. 6, which also presents the small polaron-conduction mechanism. The electrical conductivity increases with temperature through a maximum, then decreases. The transition temperatures of the electrical conductivity for $Ba_xSr_{1-x}Co_{0.8}Fe_{0.2}O_{3-\delta}$ samples are obviously different. This temperature increases with the Ba content in $Ba_xSr_{1-x}Co_{0.8}Fe_{0.2}O_{3-\delta}$, suggesting that Ba-rich samples have a high oxygen-loss temperature and thus high structural stability.

The conductivity of BSCF materials generally decreases with increasing Ba content and reaches a minimum at $x = 0.5$. The electrical conductivity of a $Ba_{0.3}Sr_{0.7}Co_{0.8}Fe_{0.2}O_{3-\delta}$ sample is obviously higher than that of other samples at low temperatures. This is ascribable to the difference in radius between Ba^{2+} and Sr^{2+} ions, Ba^{2+} having a much larger ionic radius than Sr^{2+} ($r_{Ba^{2+}} = 1.75$ Å, $r_{Sr^{2+}} = 1.58$ Å). With increasing Ba content, the unit cells become distorted (as indicated in Fig. 3), which will result in distortion energy. This will be unfavorable to the transfer of charge carriers in the materials and this negative effect reaches a maximum as the Ba/Sr ratio increases to 1.

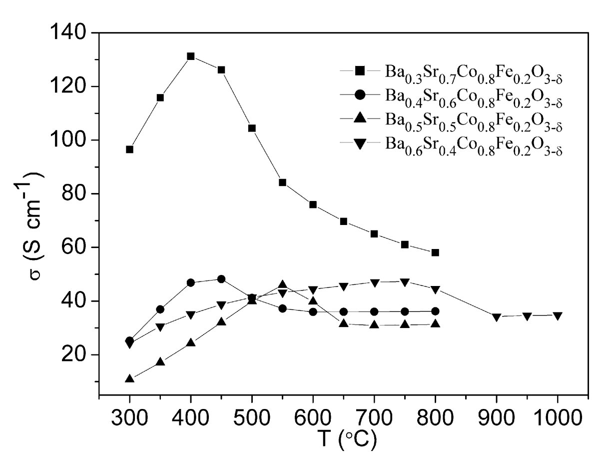

Fig. 6. Temperature dependence of electrical conductivity of $Ba_xSr_{1-x}Co_{0.8}Fe_{0.2}O_{3-\delta}$ samples with different A-site compositions.

On the other hand, the electrical conductivity is proportional to the concentration of charge carriers. For $Ba_xSr_{1-x}Co_{0.8}Fe_{0.2}O_{3-\delta}$, the decreasing electrical conductivity indicates the diminishing electron–hole concentration. Based on defect chemistry theory, the electron holes are obtained by the valence change of B-site ions. The passive effect of elemental Ba on the valence change is possibly related to its large ionic radius. For materials with perfect cubic perovskite structure (ABO_3), the ionic radii of all the elements obey

$$(r_A + r_O) = \sqrt{2}(r_B + r_O) \quad (4)$$

where r_A, r_B and r_O are the effective ionic radii of the A-site element, B-site element and oxygen, respectively. The tolerance factor t which is used to evaluate the structural stability can be calculated according to

$$t = \frac{r_A + r_O}{\sqrt{2}(r_B + r_O)} \quad (5)$$

when $t = 1$, the material reaches a standard cubic perovskite structure; this can be maintained when $0.88 \leq t \leq 1.09$ [22]. The structural stability requires that the value of t is as close as possible to 1. For $Ba_xSr_{1-x}Co_{0.8}Fe_{0.2}O_{3-\delta}$ ($x = 0.3, 0.4, 0.5, 0.6$) materials, t has a minimum value of 1.014 when $x = 0.3$ and the B-site ions are all in the trivalent state. When the Ba content increases, the effective ionic radii of the A-site elements will increase accordingly, leading to an increase of t largely deviating from 1. In order to keep the structural stability of cubic perovskite BSCF, the t-value tends to be small during the structure-formation process. Therefore, the effective ionic radii of B-site elements should be as large as possible, implying a large number of B-site ions in a low valence state. As a result, the electron–hole concentration decreases, leading to a lower electrical conductivity. According to the charge-compensation principle, the formation of oxygen vacancies is promoted in Ba-rich samples, which will lead to high ionic conductivity. Shao et al. also revealed that the introduction of Ba into $Sr(Co_{0.8}Fe_{0.2})O_{3-\delta}$ could suppress the valence change of the B-site ions from +3 to +4 [23].

3.4. Thermal-cycling stability of electrical conductivity in BSCF

Considering the durability requirement of SOFCs, the thermal-cycling stability of the cathode material's electrical conductivity is very important for good cell performance. Considering the ionic and electronic conductivities of BSCF materials, two samples of $Ba_{0.6}Sr_{0.4}Co_{0.8}Fe_{0.2}O_{3-\delta}$ and $Ba_{0.5}Sr_{0.5}Co_{0.8}Fe_{0.2}O_{3-\delta}$ were selected to investigate the cyclic performance. The process of heating a sample to each designated temperature for electrical-conductivity measurement and then cooling down to room temperature in a furnace is defined as the 1st cycle. For the same sample, the following repeated two processes are defined as the 2nd and 3rd cycles. Figs. 7 and 8 show the cyclic electrical conductivity of two samples as a function of temperature. The samples present a similar change in the behavior of the electrical conductivity during thermal cycling. The electrical conductivity in the low-temperature range clearly decreases in the second cycle, but is almost unchanged in the third cycle. The decrease of electrical conductivity after the initial thermal cycle indicates that the charge-carrier (electron holes) concentration decreases during the thermal-cycling process. This is probably related to the thermal history of the samples.

At high temperatures, the oxygen-loss reaction (3) takes place in the materials. The generated electrons are captured by the electron holes, which results in the annihilation of a certain amount of electron holes. From the thermodynamic point of view, the lost oxygen will return to the materials during the cooling process when the cooling rate is slow enough. Then reaction (6) will occur, and the lost electron holes will be regenerated:

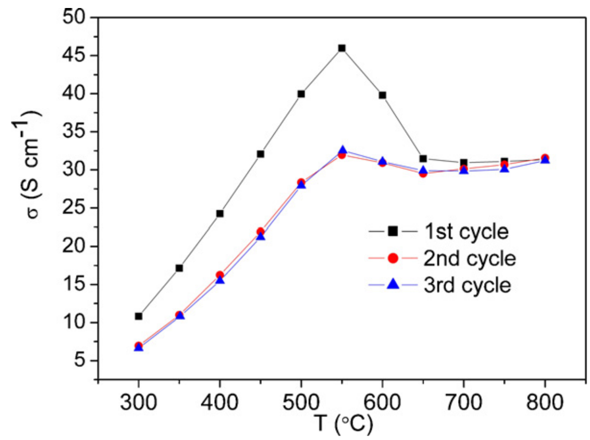

Fig. 7. Thermal cycling stability of $Ba_{0.5}Sr_{0.5}Co_{0.8}Fe_{0.2}O_{3-\delta}$ sample.

$$\frac{1}{2}O_2(g) + V_O^{\bullet\bullet} = O_O^{\times} + 2h^{\bullet} \quad (6)$$

The electrical conductivity will recover after this equilibrated thermal cycling. When the cooling rate is fast, however, reaction (6) will not be able to reach equilibrium. This will result in a lower electron–hole concentration and thus lower electrical conductivity at low temperatures. In these experiments, the sintering furnace had a lower cooling rate ($2\,^{\circ}C\,min^{-1}$), while the furnace for the electrical-conductivity measurement showed a faster cooling rate ($5\,^{\circ}C\,min^{-1}$). Therefore, the as-prepared samples exhibit relatively higher electrical conductivity (1st cycle), whereas the samples show relatively lower electrical conductivity after cycling (2nd and 3rd cycles) in the furnace for electrical-conductivity measurement. Due to their similar thermal histories, each sample presents similar conductivity on the 2nd and 3rd cycles. It is worthwhile to note that the electrical conductivity in the high-temperature range remains constant for all the investigated cycles. This suggests that a thermodynamic equilibrium state is reached at high temperatures for all the cycled samples. The concentrations of oxygen vacancies and electron holes are constant in this temperature range regardless of the thermal-cycling history.

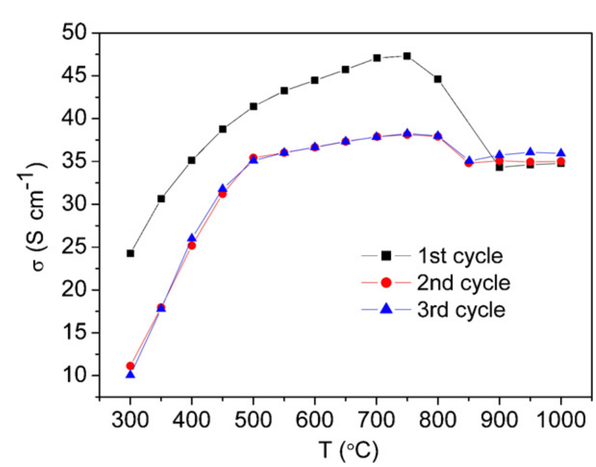

Fig. 8. Thermal cycling stability of $Ba_{0.6}Sr_{0.4}Co_{0.8}Fe_{0.2}O_{3-\delta}$ sample.

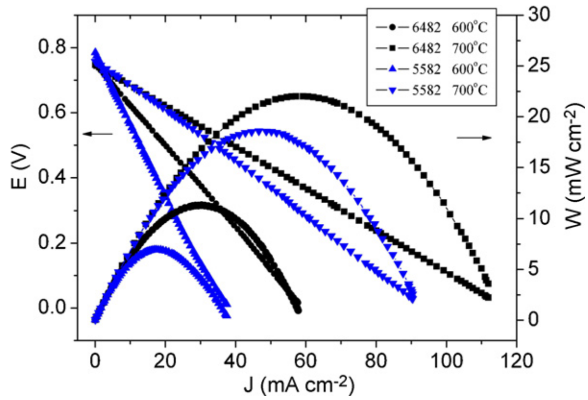

Fig. 9. Cell performance with $Ba_{0.5}Sr_{0.5}Co_{0.8}Fe_{0.2}O_{3-\delta}$ (5582) and $Ba_{0.6}Sr_{0.4}Co_{0.8}Fe_{0.2}O_{3-\delta}$ (6482) as cathode materials at different temperatures.

3.5. Cell performance of BSCF

$Ba_{0.6}Sr_{0.4}Co_{0.8}Fe_{0.2}O_{3-\delta}$ and $Ba_{0.5}Sr_{0.5}Co_{0.8}Fe_{0.2}O_{3-\delta}$ were selected as cathode materials to compare the cathode performance, considering that the former has a high and stable conductivity at high temperatures while the latter is the frequently reported composition. Electrolyte (GDC)-supported half cells with $Ba_{0.6}Sr_{0.4}Co_{0.8}Fe_{0.2}O_{3-\delta}$ and $Ba_{0.5}Sr_{0.5}Co_{0.8}Fe_{0.2}O_{3-\delta}$ as cathode materials were assembled to test the cell performances. For comparison, mixed cathode materials, BSCF with 30 wt.% GDC electrolyte, were also evaluated. The cell performances at 600 and 700 °C are shown in Figs. 9 and 10. The power densities of all the investigated cells are apparently lower than the reported data [7]. This is a characteristic of electrolyte-supported SOFCs. The large ohmic loss caused by the thick electrolyte is the main reason for this relatively poor cell performance. The aim of this work was simply to compare the cathode performances of BSCF materials with different chemical compositions.

The power densities of the investigated half cells increase obviously with temperature, mainly because of the decreased electrolyte resistance and the improved catalytic activation of the cathode materials at high temperatures. Compared with $Ba_{0.5}Sr_{0.5}Co_{0.8}Fe_{0.2}O_{3-\delta}$-based cathode materials, $Ba_{0.6}Sr_{0.4}Co_{0.8}Fe_{0.2}O_{3-\delta}$-based ones exhibit better cell power density. This is mainly due to the relatively higher electrical conductivity of $Ba_{0.6}Sr_{0.4}Co_{0.8}Fe_{0.2}O_{3-\delta}$ at intermediate temperatures (600–800 °C). The high electrical conductivity promotes the transportation of charge carriers and thus accelerates the cathode reaction. The addition of GDC to BSCF cathode materials significantly improves the cell performance, probably due to the high oxygen ionic conductivity of the GDC component, which prompts the diffusion of oxygen ions in the cathode material. For the cell with $Ba_{0.6}Sr_{0.4}Co_{0.8}Fe_{0.2}O_{3-\delta}$ as the cathode material, the highest power density at 700 °C is 23 mW cm^{-2}, which is very close to that of the cell with a $Ba_{0.5}Sr_{0.5}Co_{0.8}Fe_{0.2}O_{3-\delta}$ + GDC cathode. This implies that $Ba_{0.6}Sr_{0.4}Co_{0.8}Fe_{0.2}O_{3-\delta}$ has higher ionic conductivity than $Ba_{0.5}Sr_{0.5}Co_{0.8}Fe_{0.2}O_{3-\delta}$, which is consistent with the analysis in Section 3.3. The half cell with $Ba_{0.6}Sr_{0.4}Co_{0.8}Fe_{0.2}O_{3-\delta}$ + GDC as cathode material displays a power density of 30 mW cm^{-2} at 700 °C.

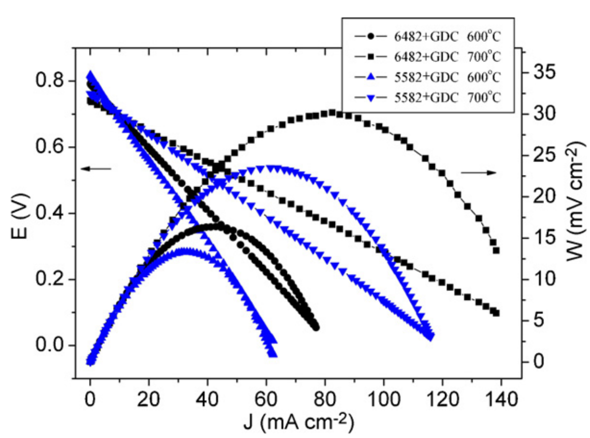

Fig. 10. Cell performance with ($Ba_{0.6}Sr_{0.4}Co_{0.8}Fe_{0.2}O_{3-\delta}$ + GDC) and ($Ba_{0.5}Sr_{0.5}Co_{0.8}Fe_{0.2}O_{3-\delta}$ + GDC) mixtures as cathode materials at different temperatures.

4. Conclusions

The solid-solution ranges of A- and B-site elements in BSCF have been investigated. Compared to A-site elements, B-site elements show a wide solution range in BSCF. With increasing Ba content in A sites or Co content in B sites, the lattice parameter *a* of BSCF increases progressively. The former is mainly due to the larger ionic radius of Ba^{2+} compared to Sr^{2+}, while the latter is attributable to the poorer ability of Co ions to change valency from trivalent to tetravalent compared with Fe ions. $Ba_xSr_{1-x}Co_yFe_{1-y}O_{3-\delta}$ presents p-type polaron hopping controlled conduction behavior. The electrical conductivity of $Ba_xSr_{1-x}Co_yFe_{1-y}O_{3-\delta}$ decreases with an increase of Ba or Co content, which is strongly related to the preferential formation of trivalent B-site ions in Ba- or Co-rich samples. Accordingly, the oxygen vacancy concentration should be high in these samples from electrostatic neutrality considerations. $Ba_{0.6}Sr_{0.4}Co_{0.8}Fe_{0.2}O_{3-\delta}$ exhibits relatively high electrical conductivity at intermediate temperatures and also shows a better cathode performance in the GDC-supported half cell compared with $Ba_{0.5}Sr_{0.5}Co_{0.8}Fe_{0.2}O_{3-\delta}$. The addition of GDC to a BSCF cathode could clearly improve the cathode performance. Both $Ba_{0.6}Sr_{0.4}Co_{0.8}Fe_{0.2}O_{3-\delta}$ and $Ba_{0.5}Sr_{0.5}Co_{0.8}Fe_{0.2}O_{3-\delta}$ samples present good thermal-cycling stability in their electrical conductivity.

Acknowledgements

This research was kindly supported by the National Natural Science Foundation of China (no. 50672009) and 863 Program of National High Technology Research Development Project of China (no. 2006AA11A189).

References

[1] K.C. Wincewicz, J.S. Cooper, J. Power Sources 140 (2005) 280–296.
[2] N.P. Brandon, B. Skinner, B.C.H. Steele, Ann. Rev. Mater. Res. 33 (2003) 183–213.
[3] R. Doshi, V.L. Richards, J.D. Carter, X.P. Wang, M. Krumpelt, J. Electrochem. Soc. 146 (1999) 1273–1278.
[4] H. Ullmann, N. Trofimenko, F. Tietzb, D. Stoever, A. Ahmad-Khanlou, Solid State Ionics 138 (2000) 79–90.
[5] L.W. Tai, M.M. Nasrallah, H.U. Anderson, D.M. Sparlin, S.R. Sehlin, Solid State Ionics 76 (1995) 259–271.
[6] L.W. Tai, M.M. Nasrallah, H.U. Anderson, D.M. Sparlin, S.R. Sehlin, Solid State Ionics 76 (1995) 273–283.
[7] Z.P. Shao, S.M. Haile, Nature 431 (2004) 170–173.
[8] Q.S. Zhu, T.A. Jin, Y. Wang, Solid State Ionics 177 (2006) 1199–1204.
[9] J. Peña-Martínez, D. Marrero-López, J.C. Ruiz-Morales, B.E. Buerqler, P. Nunez, L.J. Gauckler, Solid State Ionics 177 (2006) 2143–2147.
[10] N. Ai, Z. Lu, K.F. Chen, X.Q. Huang, B. Wei, Y.H. Zhang, S.Y. Li, X.S. Xin, X.Q. Sha, W.H. Su, J. Power Sources 159 (2006) 637–640.
[11] Z.S. Duan, M. Yang, A.Y. Yan, Z.F. Hou, Y.L. Dong, Y. Chong, M.J. Cheng, W.S. Yang, J. Power Sources 160 (2006) 57–64.
[12] Q.L. Liu, K.A. Khor, S.H. Chan, J. Power Sources 161 (2006) 123–128.
[13] H. Ikawa, K. Shima, T. Taniguchi, K. Urabe, O. Fukunaqa, J. Mizusaki, Solid State Ionics 35 (1989) 217–222.
[14] Y. Suzuki, T. Takahashi, N. Nagae, Solid State Ionics 3–4 (1981) 483–487.

[15] X. Huang, H. Zhao, W. Shen, W. Qiu, W. Wu, J. Phys. Chem. Solids 67 (2006) 2609–2613.
[16] R.D. Shannon, Acta Crystallogr. A32 (1976) 751–766.
[17] I.D. Brown, Acta Crystallogr. B53 (1997) 381–393.
[18] B. Wei, Z. Lu, X. Huang, M. Liu, N. Li, W. Su, J. Power Sources 176 (2008) 1–8.
[19] J.W. Stevenson, T.R. Armstrong, R.D. Carneim, L.R. Pederson, W.J. Weber, J. Electrochem. Soc. 143 (1996) 2722–2729.
[20] J.B. Goodenough, J. Appl. Phys. 37 (1966) 1415–1422.
[21] C.Y. Huang, T.J. Huang, J. Mater. Sci. 37 (2002) 4581–4587.
[22] Y. Chen, D.J. Lan, Q. Chen, D.Q. Xiao, J.Q. Zhu, Chin. High Technol. Lett. 16 (2006) 1043–1046.
[23] Z.P. Shao, G.X. Xiong, J.H. Tong, H. Dong, W.S. Yang, Sep. Purif. Technol. 25 (2001) 419–429.